Near-infrared imaging of demineralization on the occlusal surfaces of teeth without the interference of stains

Chung Ng
Elias C. Almaz
Jacob C. Simon
Daniel Fried
Cynthia L. Darling

Near-infrared imaging of demineralization on the occlusal surfaces of teeth without the interference of stains

Chung Ng, Elias C. Almaz, Jacob C. Simon, Daniel Fried,* and Cynthia L. Darling
University of California, San Francisco, California, United States

Abstract. Most new caries lesions are found in the pits and fissures of the occlusal surface. Radiographs have extremely low sensitivity for early occlusal decay, and by the time the lesion is severe enough to appear on a radiograph, it typically has penetrated well into the dentin and surgical intervention is required. The occlusal surfaces are often heavily stained, and visual and tactile detection have poor sensitivity and specificity. Previous near-infrared imaging studies at wavelengths beyond 1300 nm have demonstrated that stains are not visible and demineralization on the occlusal surfaces can be viewed without interference from stains. The objective of our study is to determine how the contrast between sound and lesion areas on occlusal surfaces varies with wavelength from the visible to 2350 nm and determine to what degree stains interfere with that contrast. The lesion contrast for reflectance is measured in 55 extracted teeth with suspected occlusal lesions from 400 to 2350 nm employing silicon and indium gallium arsenide imaging arrays. In addition, the lesion contrast is measured on 25 extracted teeth with suspected occlusal lesions from 400 to 1600 nm in reflectance and from 830 to 1400 nm in transillumination before and after stains are removed using a ultrasonic scaler. The highest lesion contrast in reflectance is measured at wavelengths >1700 nm. Stains interfere significantly at wavelengths <1150 nm (400 to 1150) for both reflectance and transillumination measurements. Our study suggests that the optimum wavelengths for imaging decay in the occlusal surfaces are >1700 nm for reflectance (1700 to 2350 nm) and near 1300 nm (1250 to 1350 nm) for transillumination. © *The Authors. Published by SPIE under a Creative Commons Attribution 4.0 Unported License. Distribution or reproduction of this work in whole or in part requires full attribution of the original publication, including its DOI.* [DOI: 10.1117/1.JBO.24.3.036002]

Keywords: near-infrared imaging; caries detection; dental; reflectance and transillumination imaging; stains.

Paper 180669R received Dec. 15, 2018; accepted for publication Feb. 5, 2019; published online Mar. 4, 2019.

1 Introduction

More than 15 years ago, it was discovered that enamel is highly transparent in the near-infrared (NIR) beyond 1300 nm[1,2] (Fig. 1). Therefore, the NIR is well-suited for imaging lesions on both proximal and occlusal surfaces. Innovative imaging configurations such as occlusal transillumination and cross-polarization reflectance imaging can be used to image lesions on both occlusal and proximal surfaces.[5,6] The scattering coefficient of enamel is 20 to 30 times higher in the visible versus the NIR at 1300 nm providing high contrast of demineralization in the NIR.[2,3] NIR imaging allows greater diagnostic capabilities than the current standard of bitewing radiographs for both inter-proximal and occlusal carious lesions.[1,5–11] Hyperspectral NIR imaging studies have also been carried out to identify caries lesions.[12–14] Since those seminal studies, multiple commercial NIR clinical imaging devices have been introduced: CariVu (Dexis, Hatfield, Pennsylvania), which uses NIR occlusal transillumination with 780-nm light,[15,16] and the Vistacam IX (PROXI) from Durr Dental (Bietigheim-Bissingen, Germany), which uses NIR reflectance at 850 nm.[17] For caries detection schemes operating in the visible range such as fiber-optic transillumination[18–23] and the optical caries monitor,[24] along with fluorescence-based methods, stains interfere and may produce false positives.[25–38] Both *in vitro* and *in vivo* studies show that stains completely mask demineralization in the pits and

fissures.[39] The highly conjugated molecules such as melanin and porphyrins produced by bacteria and those found in food dyes accumulate in dental plaque.[40] They are responsible for the pigmentation in the visible range and do not absorb light beyond 1200 nm.[41–43]

The lesion contrast for reflectance is defined as $(I_L - I_S)/I_L$, where the intensity of the reflected or backscattered light from the lesion is I_L and that from the surrounding sound enamel is I_S. The lesion contrast for reflectance is highest at NIR wavelengths coincident with higher water absorption and low light scattering. The lesion contrast was significantly higher ($P < 0.05$) for NIR reflectance imaging at 1450 and 1600 nm than it was for NIR reflectance imaging at 1300 nm, visible reflectance imaging, and quantitative light fluorescence (QLF).[44] The markedly higher contrast at 1450- and 1600-nm wavelengths, coincident with higher water absorption, suggests that these wavelengths are better suited than 1300 nm for imaging early/shallow demineralization on tooth surfaces, and they manifest greater intensity and contrast variation with lesion depth and severity.[45] Imaging at shorter NIR wavelengths near 830 nm was investigated more than a decade ago.[7] The 830-nm system was capable of higher performance than visible systems, but the contrast was significantly lower than that attainable at 1300 nm and simulated lesions could not be imaged through the full enamel thickness due to greater light scattering.[7] In addition, it appears that stains are still visible at the shorter NIR imaging systems, where commercial systems are now operating.[15,16]
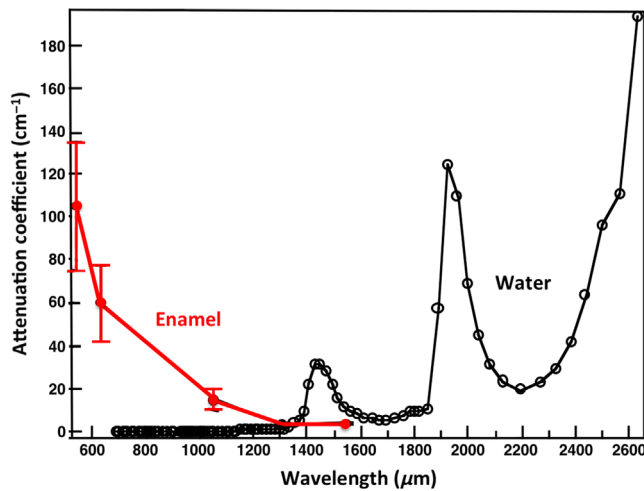
Fig. 1 The attenuation coefficient for dental enamel (red) and the absorption coefficient of water (black) in the visible and NIR.[2–4]

Studies indicate that light scattering in dental enamel decreases with increasing wavelength, and increased water absorption decreases the backscattered light (reflectance) from sound tooth structure.[3,39,45] Therefore, higher contrast between sound and demineralized enamel is expected at longer NIR wavelengths beyond 1700 nm and preliminary reflectance measurements support this hypothesis. Hyperspectral images of Zakian et al.[14] showed the tooth continuing to get darker and darker with increasing wavelength. The magnitude of absorption by water at 1940 nm (120 cm^{-1}) is 4 times higher than at 1450 nm (29 cm^{-1})[4] (see Fig. 1). Higher contrast translates to higher diagnostic performance and earlier detection of demineralization. The spectral response of indium gallium arsenide (InGaAs) can be extended well beyond 1700 nm to reach the strong water absorption band at 1940 nm by removing the underlying indium phosphide substrate on which the InGaAs is deposited. In this study, an extended range InGaAs camera sensitive from 1000 to 2350 nm was used. Even though light scattering in enamel is at a minimum in the NIR, light scattering in sound dentin is high. At wavelengths highly absorbed by water, i.e., 1450 and 1940 nm, deeply penetrating light is absorbed by the water in the surrounding/underlying sound enamel and dentin, thus increasing lesion contrast.

The purpose of this study is to determine the influence of tooth staining found in the pits and fissures of occlusal tooth surfaces on the image contrast of reflectance and transillumination measurements at NIR wavelengths and determine if higher lesion contrast is attainable at wavelengths >1700 nm. We hypothesize that reduced interference from stains, lower light scattering from sound enamel, and increased absorption by water at longer wavelengths will yield higher contrast of caries lesions on tooth occlusal surfaces. Higher lesion contrast translates to higher diagnostic performance and earlier detection.

2 Materials and Methods

2.1 Sample Preparation

Eighty human teeth with suspected noncavitated occlusal surface caries, International Caries Detection and Assessment System scores of 1 to 3, were collected (Committee on Human Research approved) and sterilized with gamma radiation.

All teeth were brushed with a dentifrice to remove any loose debris and biofilm, and they were mounted in black orthodontic acrylic blocks. All teeth that were included in the study had stains that were visually apparent on the occlusal surface after brushing. Samples were stored in a moist environment of 0.1% thymol to maintain tissue hydration and prevent bacterial growth.[15] The samples were split into two groups and the first set of samples ($n = 55$) was used to assess the wavelength dependence on the lesion contrast in reflectance from 400 to 2350 nm. QLF measurements were also carried out for comparison. An extended range NIR InGaAs imaging array was used in this study, which was sensitive out to 2350 nm. These teeth were sectioned after imaging and assessed with polarized light microscopy (PLM) and transverse microradiography (TMR) to confirm lesion presence in dentin. Eleven of the teeth had lesions confined to the outer half of enamel (E1), twenty-six teeth had lesions penetrating to the inner half of enamel (E2), and lesions in the remaining fourteen teeth penetrated into the dentin (D).

A second group of 25 teeth were used to assess the influence of stain on the lesion contrast. The lesion contrast was measured from 400 to 1600 nm in reflectance and from 400 to 1380 nm in occlusal transillumination measurements before and after stain removal. A special germanium (Ge)-enhanced silicon (Si) imaging array was used, which was capable of operating from 400 to 1600 nm so that the same imager could be used for all the measurements. Wavelengths beyond 1380 nm were not used for occlusal transillumination because of increased water absorption. Stain was removed with an ultrasonic scaler and the teeth were not sectioned after removal.

2.2 Near-Infrared Reflectance Measurements 400 to 2350 nm (Group 1 – n = 55 Teeth)

Visible color images of the samples were acquired using a USB microscope, Model AM7915MZT from AnMO Electronics Corporation (New Taipei City, Taiwan) with extended depth of field and cross polarization. The digital microscope captures 5 megapixel (2952 × 1944) color images.

The second setup of Fig. 2 was used for reflectance measurements at 400 to 1000 nm and from 900 to 2350 nm using the light sources and NIR cameras described later. The tooth occlusal surface was illuminated by the light sources at a 30-deg angle to the surface normal of the tooth occlusal surface as shown in Fig. 2. Crossed polarizers were used to remove specular reflection (glare).

A DMK-3002–IR NIR sensitive CCD camera (Imaging Source, Charlotte, North Carolina) equipped with an Infinity Infinimite lens was used to acquire 400- to 1000- and 850-nm images. A 150-W fiber-optic illuminator FOI-1 (E Licht Company, Denver, Colorado) coupled to an adjustable aperture was used as a light source and an 850-nm filter with a 70-nm bandwidth was used for the 850-nm images.

A Xenics (Leuven, Belgium) Model Xeva-2.35-320 extended range InGaAs camera sensitive from 900 to 2350 nm (320 × 240 pixel) with a Navitar SWIR optimized $f = $ 35-mm lens ($f/1.4$) was used to acquire images from 1000 to 2350 nm. A stabilized Tungsten IR light source, Model SLS202, from Thorlabs (Newton, New Jersey) with a peak output at 1500 nm and collimating optics was used. Several bandpass [BP wavelength (bandwidth)] and longpass [LP wavelength] filters were used to select wavelength intervals in the NIR,
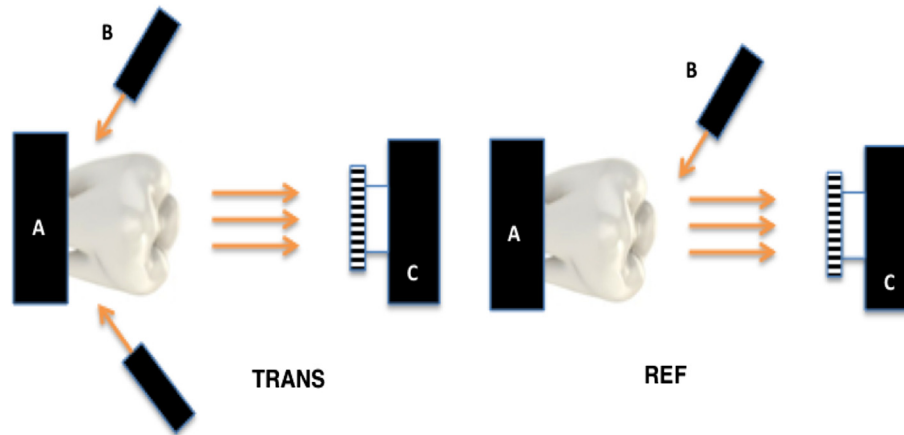
Fig. 2 Imaging configurations for (TRANS) NIR occlusal transillumination and (REF) cross-polarized NIR reflectance with (A) tooth, (B) light source, and (C) imaging camera.

including BP850(90), BP1150(78), BP1300(90), BP1460(85), BP1675(90), and LP1695.

All image analysis was carried out using Igor Pro software, Wavemetrics (Lake Oswego, Oregon). Intensity values (I) in arbitrary units with a bit density of 10 bits (0 to 1024) were recorded from each camera. An area of at least 500 pixels was chosen in the area of most severe staining and demineralization for the lesion intensity (I_L) and an equivalent area of sound enamel was chosen for the sound intensity (I_s). The darkest area in the color (visible light) image was used to demarcate the most severely stained area. The following formula was used to calculate the lesion contrast for reflection $(I_L - I_S)/I_L$, which varies from 0 to 1 for positive contrast, where 1 is the maximum achievable contrast and 0 is no contrast. In reflectance, demineralization increases I_L while absorption by stains decreases I_L. Since we are interested in detecting demineralization, large positive differences between I_L and I_S are desirable for caries detection. At shorter wavelengths, the high absorption by stains masks the demineralization and the contrast becomes negative, and in this case, the contrast is no longer bound between 0 and 1. Negative contrast is not meaningful and should not be compared to positive contrast values, i.e., the negative contrast can approach infinity. Repeated measures one-way analysis of variance (ANOVA) followed by the Tukey–Kramer *post-hoc* multiple comparison test were used to compare the contrast measurements between wavelengths using the statistical software Prism from GraphPad (San Diego, California).

2.3 Quantitative Light Fluorescence

QLF images were acquired using a USB microscope with 5 blue light-emitting diodes (LEDs) and a 510-nm LP filter, Model AM4115TW-GFBW from BigC (Torrance, California). Fluorescence intensity values were measured for the same lesion and sound enamel areas for the 55 samples in Sec. 2.2. However, QLF utilizes fluorescence loss so the intensity of sound enamel is higher than stained and demineralized enamel and the following formula for contrast was used $(I_S - I_L)/I_S$, where I_L is the intensity of the fluorescence from lesion areas and I_S is the fluorescence from sound areas. A paired *t*-test (two-tailed) was used to compare the lesion contrast for fluorescence (QLF) and the highest lesion contrast measured with NIR reflectance.

2.4 Near-Infrared Reflectance Measurements (400 to 1600 nm) and Near-Infrared Transillumination (830 to 1380 nm) before and after Stain Removal (Group 2 – n = 25 Teeth)

A NoblePeak Vision Triwave Imager, Model EC701 (Wakefield, Massachusetts) was used, which employs a Ge-enhanced complementary metal–oxide–semiconductor focal plane array sensitive in the visible and NIR from 400 to 1600 nm with an array of 640×480 pixels and a 10-μm pixel pitch. An Infinimite™ video lens (Infinity, Boulder, Colorado) was attached to the Triwave imager. Light from a 150-W fiber-optic illuminator FOI-1 (E Licht Company, Denver, Colorado) coupled to an adjustable aperture and several BP and LP filters were used to provide different spectral distributions of NIR light. The following filters: BP830(70), BP1150(78), BP1300 (90), BP1380(90), and LP1500 (1500 to 1600 nm) were used for the reflectance and transillumination imaging configurations as shown in Fig. 2. Transillumination images of natural teeth with stains on the occlusal surfaces were acquired using the first setup as shown in Fig. 2.[14,15] For occlusal transillumination, NIR wavelengths were delivered by a low-profile fiber optic with dual-line lights, Model P39-987 (Edmund Scientific, Barrington, New Jersey) with each light line directed at the cementum–enamel junction (CEJ) beneath the crown on the buccal and lingual sides of each tooth. The fiber-optic line lights were set at a downward angle of ∼20 deg and directed just above the CEJ. The angle and position were extremely important. If the light is directed too high on the tooth or at an upward angle, the light does not enter the dentin of the crown and the contrast of the lesion is greatly reduced, i.e., the light has to be directed under the lesion. For reflectance, the second setup in Fig. 2 was used with the Triwave imager and the 150-W FOI-1 fiber-optic illuminator.

A region of the most severely stained area of each tooth was imaged using both reflectance and transillumination before and after stain removal with a Varios 350 Lux ultrasonic scaler from NSK (Kanuma, Japan). The darkest area in the visible image was used to demarcate the most severely stained area. The lateral surface of the scaling tip was adapted to the tooth and applied in brief strokes at sites with extrinsic staining. The transillumination contrast formula used was $(I_S - I_L)/I_S$ and the reflectance contrast formula used was $(I_L - I_S)/I_L$ for positive contrast. For positive contrast, the contrast varies from 0 to 1.

Repeated measures ANOVA followed by the Tukey–Kramer *post-hoc* multiple comparison test were used to compare the contrast measurements between groups for reflectance and transillumination before and after removal.

2.5 Polarized Light Microscopy and Transverse Microradiography

After all diagnostic images were captured, samples were serially sectioned into ∼200-μm-thick mesiodistal slices using a linear precision saw, Isomet 5000 (Buehler, Lake Bluff, Illinois). Thin sections were examined by PLM and TMR.

PLM was used to examine the thin sections using a Meiji Techno RZT microscope (Saitama, Japan) with an integrated digital camera, Canon EOS Digital Rebel XT (Tokyo, Japan). Sample sections 200-μm thick were imbibed in deionized water and examined in the bright-field mode with crossed polarizers and a red I plate with 550-nm retardation.

PLM is reliable for assessing demineralization in enamel since sound enamel weakly scatters light and demineralization scrambles the polarization causing lesion areas to appear dark; however, it is more difficult to interpret in dentin due to the very high light scattering in sound dentin. Therefore, we used TMR to confirm lesion penetration into dentin for those samples where the demineralization appeared to reach the dentin. A custom-built digital microradiography system was used to measure the volume percent mineral content in the areas of demineralization on the tooth sections.[46] High-resolution microradiographs were taken using Cu Kα radiation from a Philips 3100 x-ray generator and a Photonics Science FDI x-ray digital imager, Microphotonics (Allentown, Pennsylvania). The x-ray digital imager consisted of a 1392×1040 pixel interline CCD directly bonded to a coherent microfiber-optic coupler that transfers the light from an optimized gadolinium oxysulfide scintillator to the CCD sensor. The pixel resolution was 2.1 μm and the images were acquired at 10 frames per second. A high-speed motion control system with Newport UTM150 and 850G stages and an ESP 300 controller coupled to a video microscopy and a laser targeting system was used for precise positioning of the samples in the field of view of the imaging system.

3 Results

Examples of reflectance images taken from one of the samples with both light stain and occlusal demineralization are shown in Fig. 3. The visible (color) light image in Fig. 3(a) shows white areas in the grooves indicative of demineralization and some darker discolored areas in the grooves due to stains. The small red and green boxes in Fig. 3(a) demarcate the areas on the tooth surface used to calculate I_L and I_S, respectively. The QLF image in Fig. 3(c) shows dark areas that correspond to lesion areas. NIR reflectance images are shown in the last four images of Fig. 3 and areas of demineralization all appear whiter than the surrounding sound enamel. The tooth was sectioned at the position of the two thin black lines shown in Fig. 3(a) and PLM and TMR images of that cut section are shown in Figs. 3(b) and 3(d), respectively. The darker areas in the PLM and TMR images indicate areas of demineralization, and there is extensive demineralization in the occlusal groove penetrating to the dentin.

A second tooth with extensive staining and minimal demineralization is shown in Fig. 4. In the visible (color) image [Fig. 4(a)], the tooth looks somewhat similar to the tooth in Fig. 3 with extensive staining in fissure areas; however, there
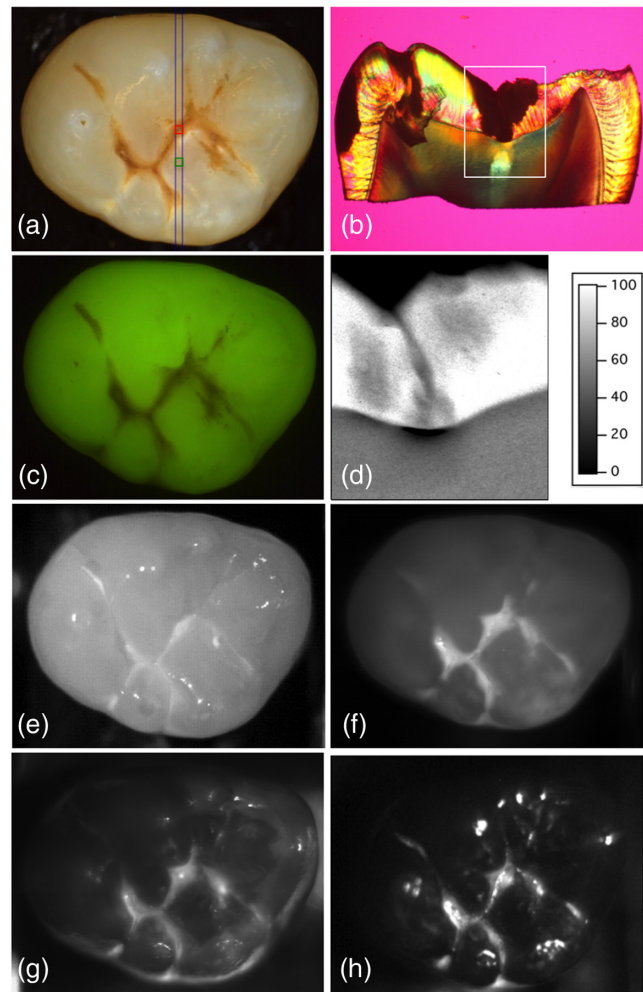

Fig. 3 Images of a tooth from group 1 with demineralization in the fissure. (a) visible (color), (b) PLM image cut at the position of the two thin blue lines in (a), (c) QLF, TMR measurements of % mineral compared to sound enamel for the region marked in the PLM image (d), NIR reflectance at (e) 850, (f) 1300, (g) 1675, and (h) 1695 to 2350 nm. The upper red and lower green boxes mark the area chosen for lesion and sound for the contrast calculations, respectively.

are no whiter areas visible indicative of demineralization. The darkest most severely stained fissure area is in the position of the small red box located in between the two thin black lines in Fig. 4(a). The small red and green boxes in Fig. 4(a) demarcate the areas on the tooth surface used to calculate I_L and I_S, respectively. The darker fissures areas in Fig. 4(a) also appear dark in the QLF image [Fig. 4(c)] and in the shorter wavelength NIR reflectance image at 850 nm [Fig. 4(e)]. The longer wavelength NIR reflectance image at 1300 nm [Fig. 4(f)] shows only very minor whiter areas indicative of demineralization in a few of the fissures; however, there is no demineralization visible in the area of the red box shown in Fig. 4(a). Beyond 1675 nm [Figs. 4(g) and 4(h)], there is still no demineralization (whiter areas) visible in the marked fissure area (red box). Note that some of the white spots around the outside of the tooth in Figs. 4(g) and 4(h) are due to specular reflection and not demineralization. High extinction ratio polarizers operating at wavelengths beyond 1700 nm have only become recently available, and the extinction ratio was lower for wavelengths beyond 1700 nm. Specular reflection changes with a slight tilt of the

tooth while the reflectivity of demineralization remains stable so the specular reflection is easily differentiated from demineralization. In addition, the intensity of specular reflection is strongly affected by rotation of the polarizer compared to the actual areas of demineralization. The tooth was sectioned at the position of the two thin black lines, and the center of the fissure in the PLM micrograph of Fig. 4(b) corresponds to the position of the red box in Fig. 4(a). The PLM micrograph shows that there is a dark mass of organic material (stain) filling the fissure; however, the fissure walls are completely intact and there is no demineralization visible on the walls. The TMR image of the same section [Fig. 4(d)] is of a higher magnification, matching the area of the white box in the PLM image of Fig. 4(b). The dark mass in the fissure is not visible in the TMR image suggesting it has a mineral density of zero and is likely organic matter, i.e., stain or noncalcified plaque. It is remarkable that it was possible to cut a section only 200-μm thick of the tooth without loss of the mass of organic matter in the fissure. In addition, the

TMR image also indicates that the walls of the fissure are intact and that there is no demineralization present.

The mean lesion contrast (reflectance) $\pm$ standard deviation (sd) for all the 55 teeth of group 1 is plotted in Fig. 5 for visible, 850-, 1150-, 1300-, 1460-, 1675-, and 1695- to 2350-nm wavelengths. The mean contrast was highly negative, -1.85 ± 2.7, for visible/NIR (400 to 1000 nm) and also negative for 850 nm. The contrast increased with increasing wavelength and was highest for 1695 to 2350 nm, where it was 0.68 ± 0.21. All the groups were significantly different from each other ($P < 0.01$). The lesion contrast for fluorescence (QLF) was 0.48 ± 0.18, which was significantly lower than the contrast at 1695 to 2350 nm. The mean lesion contrast $\pm$ sd for the early lesions (E1) of group 1 that are limited to the outer enamel ($n = 11$) is plotted in Fig. 6. The same trend with wavelength is observed although the contrast is lower for each wavelength. A similar plot of the more severe lesions of group 1 that have penetrated to dentin (D lesions, $n = 14$) also shows the same trend albeit with higher lesion contrast.
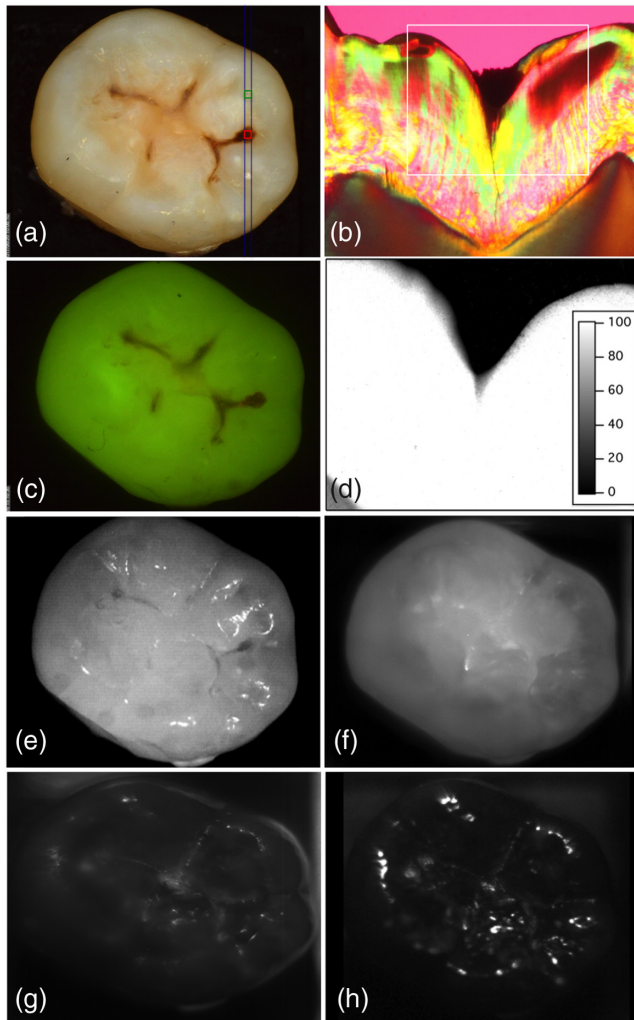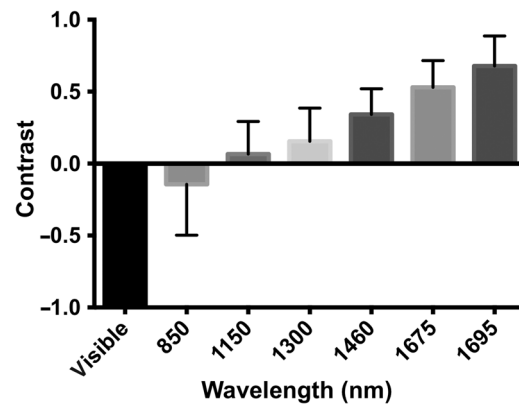

Fig. 4 Images of another tooth from group 1 without demineralization in the fissure. (a) visible (color), (b) PLM image cut at the position of the two thin blue lines in (a), (c) QLF, TMR measurements of % mineral compared to sound enamel for the region marked in the PLM image (d), NIR reflectance at (e) 850, (f) 1300, (g) 1675, and (h) 1695 to 2350 nm. Only stain is visible suspended in the occlusal pit. The lower red and upper green boxes mark the area chosen for lesion and sound for the contrast calculations, respectively.

Fig. 5 The mean lesion contrast $\pm$ sd for the 55 teeth in group 1: 400- to 1000-, 850-, 1150-, 1300-, 1460-, 1675-, and 1695- to 2350-nm wavelengths are shown. All the groups are significantly different ($P < 0.01$). The mean contrast in the visible is -1.85 ± 2.7 and extends beyond the graph.
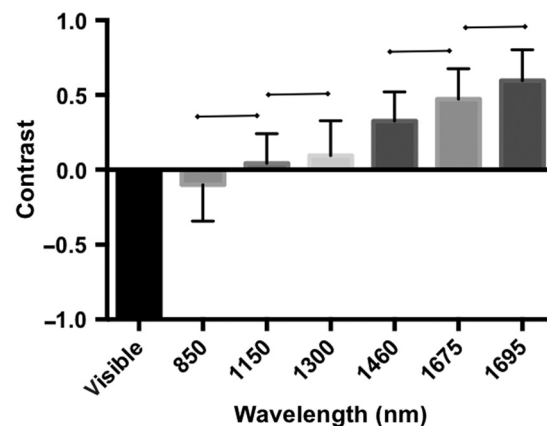

Fig. 6 The mean lesion contrast $\pm$ sd for the 11 teeth in group 1 that were limited in depth to the first half of the enamel, E lesions: 400- to 1000-, 850-, 1150-, 1300-, 1460-, 1675-, and 1695- to 2350-nm wavelengths are shown. Groups with a connecting line above are statistically similar ($P > 0.05$). The mean contrast in the visible is -1.4 ± 1.4 and extends beyond the graph.

NIR occlusal transillumination and reflectance images of tooth occlusal surfaces were acquired of a second group of 25 teeth before and after stain removal with an ultrasonic scaler. Filters centered at 830, 1150, 1300, 1380, and 1550 nm (1500 to 1600 nm) were used to segregate the NIR region for each corresponding image. Sample images of a tooth that has stained fissures with shallow demineralization present under the stain along with interproximal lesions are shown in Fig. 7 before and after stain removal. In transillumination, both the stain and demineralization appear dark. At 830 nm, most of the dark areas are removed after scaling; however, at 1380 nm, there is little change since the stain is not visible. In reflectance, the stain appears darker and the demineralization appears whiter. Note how the interproximal lesion appears dark in transillumination and white in reflectance. At 830 nm, the fissures appear very dark due to the strong absorption by the stain. At 1380 and 1550 nm, the stain is not visible and the demineralization under the stain is clearly visible as whiter areas in the fissures. The contrast of the demineralization is highest at 1550 nm. After scaling, most of the dark areas at 830 nm are no longer visible and some of the underlying demineralization can now be seen. At 1550 nm after scaling some of the whiter areas have been removed, this suggests that the scaler also removed some of the demineralization and that the demineralization present was fairly shallow.

Plots of the mean lesion contrast ± sd versus wavelength measured for the second group of 25 samples before and after stain removal are shown in Fig. 8 for NIR reflectance and NIR occlusal transillumination.

The greatest changes in contrast in the images for NIR occlusal transillumination occur at 830 and 1150 nm while there is little change at the longer wavelengths of 1300 and 1380 nm after removal of the stain. Even at 830 nm, after the aggressive use of an ultrasonic scaler to remove the stain, it was still visible in most of the samples. The magnitude of the change falls off significantly when the imaging wavelength is increased to 1150 nm. There was a significant difference ($P < 0.05$) in the change in lesion contrast before and after stain removal at 830 and 1150 nm. The change with lesion removal was smaller and was no longer significant at 1300 and 1380 nm. In contrast to reflectance, in NIR transillumination,
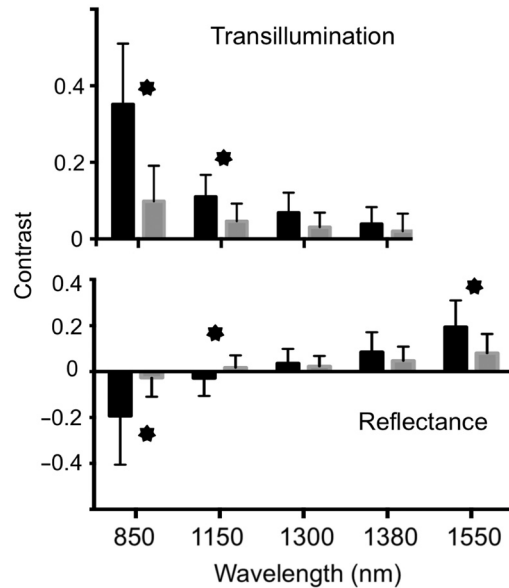
Fig. 8 The mean lesion contrast ± sd for NIR reflectance and transillumination of the 25 teeth in group 2 before and after stain removal with the cavitron. Wavelengths of 830, 1150, 1300, 1380, and 1550 nm are shown. Groups for which the contrast changed significantly ($P < 0.05$) after stain removal have an asterisk.

stain and demineralization both reduce the intensity so that it is not possible to differentiate between them.

The NIR reflectance images appear similar to those observed in NIR transillumination where the stain is visible at 830 and 1150 nm before removal and most of it vanishes after removal, although there is also some stain still visible at 830 nm after removal. Some whiter areas in the fissures due to demineralization become visible in reflectance at 1300 and 1380 nm before and after stain removal, and there are only small changes after removal. However, at 1550 nm, the demineralization is clearly visible before removal. The mean contrast decreased after stain removal indicating that the ultrasonic scaler actually removed some demineralized enamel in addition to removing the stain. For NIR reflectance, there was a significant difference in contrast before and after stain removal for 830, 1150, and 1550 nm. The contrast was negative for 830 and 1150 nm before stain removal indicating the contrast at these wavelengths was dominated by stains. The mean lesion contrast remained negative even after lesion removal at 830 nm; however, the contrast flipped to positive at 1150 nm after removal. The contrast was positive at 1300, 1380, and 1550 nm, and it decreased with stain removal as opposed to increasing with 830 and 1150 nm.

4 Discussion

The occlusal surfaces of posterior teeth typically have stains in the pits and fissures of the occlusal surface that interfere with visual diagnosis and fluorescence-based caries detection systems. Manufacturers advise thoroughly cleaning the pits and fissures before taking measurements; however, a thorough removal of all stain from the pits and fissures is obviously not feasible. In this study, it was necessary to use an ultrasonic scaler to remove most of the stains. Such an invasive system is too destructive and aggressive for clinical use, and even after use there was still sufficient stain remaining to mask the demineralization at 830 nm.
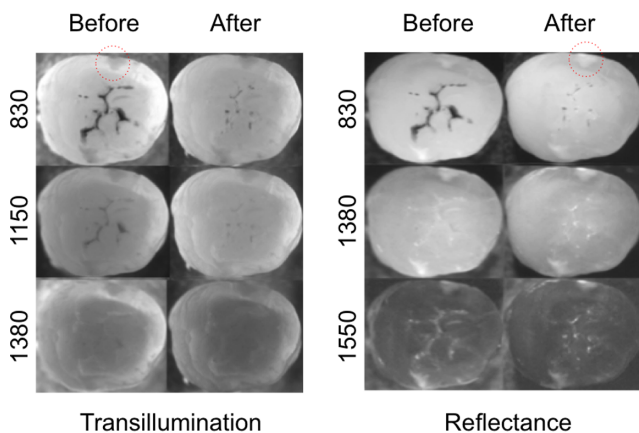

Fig. 7 Sample NIR transillumination and NIR reflectance images from a tooth of the group 2 samples before and after stain removal with the cavitron at different wavelengths. An interproximal lesion is also present on the tooth in the area of the red circle.

The lesion contrast measurements presented in Fig. 5 indicate that the lesion contrast continues to increase beyond 1700 nm (1695 to 2350 nm), where there is decreasing light scattering in the sound enamel and there is increasing light absorption by water (Fig. 1). Current NIR imaging devices on the market for caries detection operate at 780 and 850 nm, where these studies show that there is significant interference from stains. In addition, the contrast between sound and demineralized tooth structure is markedly higher at longer NIR wavelengths than it is at 850 nm. The primary disadvantage of operating at longer NIR wavelengths is that Si-based imaging technologies are only efficient at wavelengths under 1000 nm. Alterative imaging technologies such as InGaAs and Ge-enhanced Si are still expensive. Less expensive scanned NIR LED and NIR diode light sources and galvanometer or MEMS-based scanning systems are also feasible. The limited use of these more innovative semiconductors technologies is a major reason for the high cost. However, with expanded use, those prices are expected to decrease. The cost has decreased significantly in the past 10 years and the performance has increased markedly. Using the newly available extended range InGaAs imaging array sensitive beyond 1700 nm, we have demonstrated that even higher lesion contrast is attainable at longer NIR wavelengths. Imaging at longer wavelengths beyond 1700 nm may also be advantageous for assessing lesion activity by looking at the lesion contrast during drying since the longer wavelengths are more sensitive to changes in water. Since many of the caries imaging devices use fluorescence, we compared our results with QLF. QLF is highly effective for increasing image contrast on tooth surfaces since there is no interference from specular reflectance. However, QLF uses visible light for excitation and the fluorescence is in the visible range so that stains interfere with both excitation and fluorescence. Demineralization and absorption by stains increase the lesion contrast for QLF and it is not possible to differentiate between the two. Therefore, it is unreliable on tooth surfaces where stains occur. However, even with stains contributing to the positive lesion contrast in QLF, the contrast in NIR reflectance beyond 1700 nm was significantly higher. Stains are also a potential problem for the red or porphyrin-based caries detection systems that employ both blue light and red light for excitation and then image the fluorescence at longer red and NIR wavelengths since stains also interfere at 600 to 800 nm.

Using the second group of 25 teeth, it was demonstrated that at NIR wavelengths <1150 nm, the lesion contrast in the occlusal surfaces is masked by interference from stains. At 830 nm, the stain still dominated the lesion contrast in reflectance and the mean contrast was still negative even after extreme measures were taken to remove it. In transillumination at 830 nm, the lesion contrast dropped by almost a factor of 4 after removal. The contrast dropped slightly beyond 1300 nm in transillumination but that is likely due to loss of demineralization. Although we did not directly measure the depth of demineralization before and after removing the stains with the ultrasonic scaler, there is strong evidence that some of the demineralization was also removed in addition to the stains. The mean lesion contrast for reflectance increased markedly (became more positive) at 850 and 1150 nm when the stains were removed while that contrast decreased at longer wavelengths, 1300 and 1550 nm, where only demineralization contributes to lesion contrast. If there was significant reflectivity from the stains or plaque on the surface, then we would expect a reduction in the reflectance at all the NIR wavelengths. In addition, we would expect to see an increase in the lesion contrast in transillumination at wavelengths >1300 nm after removal of the stain, not a decrease as was observed. Moreover, images before and after removal for deeper areas of demineralization at 1550 nm do not show as great a change in the lesion area as seen for the tooth shown in Fig. 7. Damage occurs only near the surface of the lesion where only shallow and superficial demineralization is removed, deeper lesion areas remain intact.

This study suggests that stains on teeth interfere significantly with the lesion contrast at wavelengths shorter than 1150 nm and imaging wavelengths ranging beyond 1300 nm are not significantly influenced by the presence of stain in the pits and fissures found on occlusal surfaces. Therefore, NIR imaging performed above 1150 nm can detect early demineralization below stained surfaces. In addition, these studies show that the contrast of demineralization increases significantly at wavelengths beyond 1700 nm. Therefore, based on these and previous studies, it appears that wavelengths near 1300 nm where light scattering and water absorption are both low are best for NIR transillumination while wavelengths beyond 1700 nm where light scattering is low and water absorption is high are best for NIR reflectance measurements.

Disclosures

Acknowledgments

References

1. R. Jones et al., "Near-infrared transillumination at 1310-nm for the imaging of early dental decay," *Opt. Express* **11**(18), 2259–2265 (2003).
2. R. S. Jones and D. Fried, "Attenuation of 1310-nm and 1550-nm laser light through sound dental enamel," *Proc. SPIE* **4610**, 187–190 (2002).
3. D. Fried et al., "Nature of light scattering in dental enamel and dentin at visible and near-infrared wavelengths," *Appl. Opt.* **34**(7), 1278–1285 (1995).
4. G. M. Hale and M. R. Querry, "Optical constants of water in the 200-nm to 200-μm wavelength region," *Appl. Opt.* **12**, 555–563 (1973).
5. C. Buhler, P. Ngaotheppitak, and D. Fried, "Imaging of occlusal dental caries (decay) with near-IR light at 1310-nm," *Opt. Express* **13**(2), 573–582 (2005).
6. M. Staninec et al., "In vivo near-IR imaging of approximal dental decay at 1,310 nm," *Lasers Surg. Med.* **42**(4), 292–298 (2010).
7. G. Jones, R. S. Jones, and D. Fried, "Transillumination of interproximal caries lesions with 830-nm light," *Proc. SPIE* **5313**, 17–22 (2004).
8. C. Lee, C. L. Darling, and D. Fried, "In vitro near-infrared imaging of occlusal dental caries using a germanium enhanced CMOS camera," *Proc. SPIE* **7549**, 75490K (2010).
9. D. Fried et al., "Early caries imaging and monitoring with near-infrared light," *Dent. Clin. N. Am.* **49**(4), 771–793 (2005).
10. D. Lee, D. Fried, and C. Darling, "Near-IR multi-modal imaging of natural occlusal lesions," *Proc. SPIE* **7162**, 71620X (2009).
11. J. C. Simon et al., "Near-IR transillumination and reflectance imaging at 1300-nm and 1500–1700-nm for in vivo caries detection," *Lasers Surg. Med.* **48**(6), 828–836 (2016).

12. S. Salsone et al., "Histological validation of near-infrared reflectance multispectral imaging technique for caries detection and quantification," *J. Biomed. Opt.* **17**(7), 076009 (2012).

13. P. Usenik et al., "Automated classification and visualization of healthy and diseased hard dental tissues by near-infrared hyperspectral imaging," *Appl. Spectrosc.* **66**(9), 1067–1074 (2012).

14. C. Zakian, I. Pretty, and R. Ellwood, "Near-infrared hyperspectral imaging of teeth for dental caries detection," *J. Biomed. Opt.* **14**(6), 064047 (2009).

15. J. Kuhnisch et al., "In vivo validation of near-infrared light transillumination for interproximal dentin caries detection," *Clin. Oral Invest.* **20**(4), 821–829 (2016).

16. F. Sochtig, R. Hickel, and J. Kuhnisch, "Caries detection and diagnostics with near-infrared light transillumination: clinical experiences," *Quintessence Int.* **45**(6), 531–538 (2014).

17. A. Jablonski-Momeni, B. Jablonski, and N. Lippe, "Clinical performance of the near-infrared imaging system VistaCam iX Proxi for detection of approximal enamel lesions," *BDJ Open* **3** 17012 (2017).

18. J. Barenie, G. Leske, and L. W. Ripa, "The use of fiber optic transillumination for the detection of proximal caries," *Oral Surg.* **36** 891–897 (1973).

19. C. M. Pine, "Fiber-optic transillumination (FOTI) in caries diagnosis," in *Early Detect. Dent. Caries, Proc. 1st Annu. Indiana Conf.*, Indiana University, pp. 51–66 (1996).

20. R. D. Holt and M. R. Azeevedo, "Fiber optic transillumination and radiographs in diagnosis of approximal caries in primary teeth," *Community Dent. Health* **6**, 239–247 (1989).

21. C. M. Mitropoulis, "The use of fiber optic transillumination in the diagnosis of posterior approximal caries in clinical trials," *Caries Res.* **19**, 379–384 (1985).

22. H. Hintze et al., "Reliability of visual examination, fibre-optic transillumination, and bite-wing radiography, and reproducibility of direct visual examination following tooth separation for the identification of cavitated carious lesions in contacting approximal surfaces," *Caries Res.* **32**(3), 204–209 (1998).

23. A. Schneiderman et al., "Assessment of dental caries with digital imaging fiber-optic transillumination (DIFOTI): in vitro study," *Caries Res.* **31**, 103–110 (1997).

24. J. J. ten Bosch, H. C. van der Mei, and P. C. F. Borsboom, "Optical monitor of in vitro caries," *Caries Res.* **18**, 540–547 (1984).

25. P. E. Benson, N. Pender, and S. M. Higham, "Quantifying enamel demineralization from teeth with orthodontic brackets—a comparison of two methods. Part 2: validity," *Eur. J. Orthod.* **25**(2), 159–165 (2003).

26. E. de Josselin de Jong, A. F. Hall, and A. H. I. M. van der Linden, "QLF: a Monte Carlo simulation model," in *Early Detect. Dent. Caries, Proc. 1st Annu. Indiana Conf.*, Indiana University, pp. 91–104 (1996).

27. G. K. Stookey, "Quantitative light fluorescence: a technology for early monitoring of the caries process," *Dent. Clin. N. Am.* **49**(4), 753–770 (2005).

28. S. Tranaeus et al., "Application of quantitative light-induced fluorescence to monitor incipient lesions in caries-active children. A comparative study of remineralisation by fluoride varnish and professional cleaning," *Eur. J. Oral Sci.* **109**(2), 71–75 (2001).

29. S. Tranaeus et al., "In vivo repeatability and reproducibility of the quantitative light-induced fluorescence method," *Caries Res.* **36**(1), 3–9 (2002).

30. R. R. Alfano et al., "Human teeth with and without caries studied by laser scattering, fluorescence, and absorption spectroscopy," *IEEE J. Quantum Electron.* **20**, 1512–1516 (1984).

31. B. A. Angmar-Masson, S. Al-Khateeb, and S. Tranaeus, "Intraoral use of quantitative light-induced fluorescence detection method," in *Early Detect. Dent. Caries, Proc. 1st Annu. Indiana Conf.*, Indiana University, pp. 39–50 (1996).

32. A. Lussi, R. Hibst, and R. Paulus, "DIAGNOdent: an optical method for caries detection," *J. Dent. Res.* **83**, 80–83 (2004).

33. A. Lussi et al., "Performance and reproducibility of a laser fluorescence system for detection of occlusal caries in vitro," *Caries Res.* **33**, 261–266 (1999).

34. X. Q. Shi, S. Tranaeus, and B. Angmar-Mansson, "Comparison of QLF and DIAGNOdent for quantification of smooth surface caries," *Caries Res.* **35**(1), 21–26 (2001).

35. G. K. Stookey, "Optical methods—quantitative light fluorescence," *J. Dent. Res.* **83**, 84–88 (2004).

36. J. J. ten Bosch, "Summary of research of quanitative light fluorescence," in *Early Detect. Dent. Caries II, Proc. 4th Annu. Indiana Conf.*, Indiana University, pp. 261–279 (1999).

37. X. Q. Shi, U. Welander, and B. Angmar-Mansson, "Occlusal caries detection with Kavo DIAGNOdent and radiography: an in vitro comparison," *Caries Res.* **34**, 151–158 (2000).

38. A. G. F. Zandona et al., "An in vitro comparison between laser fluorescence and visual examination for detection of demineralization in occlusal pits and fissures," *Caries Res.* **32**(3), 210–218 (1998).

39. S. Chung et al., "Multispectral near-IR reflectance and transillumination imaging of teeth," *Biomed. Opt. Express* **2**(10), 2804–2814 (2011).

40. A. Watts and M. Addy, "Tooth discolouration and staining: a review of the literature," *Br. Dent. J.* **190**(6), 309–316 (2001).

41. G. A. Kleter, "Discoloration of dental carious lesions (a review)," *Arch. Oral Biol.* **43**, 629–632 (1998).

42. T. Sarna and R. C. Sealy, "Photoinduced oxygen consumption in melanin systems. Action spectra and quantum yields for eumelanin and synthetic melanin," *Photochem. Photobiol.* **39**, 69–74 (1984).

43. D. Fu et al., "Two-color, two-photon, and excited-state absorption microscopy," *J. Biomed. Opt.* **12**(5), 054004 (2007).

44. W. A. Fried, "High contrast reflectance imaging of simulated lesions on tooth occlusal surfaces at near-IR wavelengths," *Lasers Surg. Med.* **45**(8), 533–541 (2013).

45. J. C. Simon, "Multispectral near-IR reflectance imaging of simulated early occlusal lesions: variation of lesion contrast with lesion depth and severity," *Lasers Surg. Med.* **46**(3), 203–215 (2014).

46. C. L. Darling et al., "An automated digital microradiography system for assessing tooth demineralization," *Proc. SPIE* **7162**, 71620T (2009).

Biographies of the authors are not available.